*34th EPS Conference on Plasma Phys. Warsaw, 2 - 6 July 2007 ECA Vol.**31F**, O-4.026 (2007)*

Confinement characteristics of pellet-fuelled plasmas in MAST

M Valovič, K Axon, L Garzotti, S Saarelma, A Thyagaraja, R Akers, C Gurl, A Kirk, B Lloyd, G P Maddison, A Patel, S Shibaev, R Scannell, D Taylor, M Walsh and MAST team

EURATOM/UKAEA Fusion Association, Culham Science Centre, Abingdon, Oxfordshire OX14 3DB, U. K.

Introduction. The present consensus is that in a reactor, high edge densities cannot be achieved by gas puffing. The only technique proposed to control the density in reactor grade plasmas is injection of cryogenic pellets. The price to pay for such deeper fuel deposition is a substantial perturbation to the plasma by the pellet itself. For example for ITER, local density increase up to 50% is expected in the pellet deposition zone located at the outer 15% of the minor radius [1, 2]. Pellet-fuelled plasmas are not stationary and the pellet deposition region is in a state of permanent response to perturbations. Pellets modify the confinement physics in the outer part of the plasma and to a large extent the pellet deposition zone takes over the role from the H-mode pedestal for setting up the boundary conditions for the plasma core.

Two practical parameters, the pellet deposition radius and the post-pellet particle confinement time, provide the link between the confinement physics and the design of the pellet fuelling system necessary to maintain the required plasma density. The present paper reports on first particle confinement data of pellet fuelled-plasmas from the MAST tokamak.

Experimental conditions. The targets for pellet injection were both L-mode and H-mode plasmas with plasma current $I_p = (0.66-0.76)MA$, geometric major radius $R_{geo} = (0.8-0.87)m$, minor radius $a = (0.55-0.60)m$, elongation $\kappa = 1.8-2.1$, vacuum toroidal field at the geometric radius $B = (0.47-0.50)T$, with double null divertor configuration and line averaged density $\bar{n}_e = (1.6-7.5)\times 10^{19} m^{-3}$. H-mode plasmas were NBI heated with launched power $P_{INJ} = (1.1-3.0)MW$. The working gas is deuterium and plasmas are heated with neutral beams with energy of $\leq 65-67\,keV$. Pellets are launched from the top and they enter the plasma from the high field side (see figure 1a) [3]. Low field side launch is also possible in MAST, but not used in this study. The nominal pellet sizes are $N_{pel} = (0.6; 1.2; 2.4)\times 10^{20}$ atoms and pellet velocities are 240-450 m/s. We selected data with only those pellets which cause relatively modest plasma perturbations approaching the conditions similar to those expected in ITER.

Pellet deposition radius. Evaporation and deposition of a single pellet lasts about 2 ms. The end of this process is clearly seen as a sharp inflexion point on the interferometer signal - an interesting observation as in neutral gas and plasma shielding models (NGPS) [4] the pellet evaporation rate decreases continuously with decreasing pellet size. The pellet evaporation and the deposition process is captured in the visible bremsstrahlung emission spectrum (figure 1b) revealing the clear burst-like structure (striations) of this process. Absolute intensity of the emission indicates densities of the cold 1-2 eV [5] ablatant up to $10^{23} m^{-3}$. The high resolution (3mm) Thomson scattering system can be triggered by the pellet signal. Measured profiles show that the plasma density quickly equilibrates along the flux surfaces already during the

pellet life time. The density profile just at the end of the pellet evaporation is shown in figure 2. The inner and outer density profiles are a relatively good function of the poloidal flux coordinate as determined from magnetic equilibrium reconstruction (EFIT). This simplifies the post pellet transport analysis as one can assume that shortly after the pellet evaporation the density and temperature profiles are conventional and do not remember the 3D character of the particle source from the pellet. Evolution of the density profile during the pellet deposition cannot be explained by the simple NGPS model [4] as seen from figure 2. Agreement is achieved only if $\nabla \mathbf{B}$-drift is added which effectively spreads the pellet deposition inwards by $\sim 0.15 r/a$. The best fit is obtained with the drift distance in the form $\lambda = c_s^2 \tau_h^2 / (2R)$, where the ion sound speed c_s corresponds to temperatures of 1-2 eV and the time during which the drift is active is $\tau_h = 10 - 40 \mu s$ [6, 7, 8].

The pellet deposition could be also affected by a temporary change in micro-turbulence induced by the pellet itself. Figure 3 shows two density profiles – one before and one just after the pellet deposition as captured by the 200 Hz Thomson scattering system. It is seen that the pellet creates a distinct zone with positive density gradient $\nabla n_e > 0$ and temperature gradient $a\nabla \ln T_e$ doubled relative to its pre-pellet value. Calculations using the linear GS2 and TRANSP codes for the case in figure 3 show that at the radius of maximum increase of $a\nabla \ln T_e$ the normalised growth rates $\gamma / k_\perp^2$ of modes with wavelengths $0.08 < k_\perp \rho_i < 0.8$ (micro-tearing and ion temperature gradient) increase by a factor of 2. The stability of these modes strongly depends on the flow shearing rate ω_s which is, however, not measured in the pellet case. In the non-pellet case, ω_s is found to be of the same magnitude as that required to stabilise the long wavelength modes $\omega_s \sim \gamma (k_\perp \rho_i < 1)$ [9]. The plasma in figure 3 has also been modelled by the global nonlinear fluid code CUTIE [10]. At the radius of maximum increase of $a\nabla \ln T_e$ the relative amplitude of density fluctuations $\tilde{n}/n$ increases threefold for $0.05 < k_\theta \rho_s < 0.2$ modes and decreases for modes with $0.2 < k_\theta \rho_s < 0.4$. However, the overall turbulent transport increases, resulting in fast inward particle propagation. Note that the enhancement of micro-turbulence in the pellet deposition zone has been also obtained by the CUTIE and TRB codes when simulating JET plasmas [11]. The temporary increase of particle transport in the zone with $\nabla n_e > 0$, indicated by simulations, would be favourable for pellet deposition. Finally, the distinct zone described above could takeover the role from the pedestal for setting-up the boundary condition for transport in the plasma core in general.

Post-pellet particle confinement time. Post pellet evolution of the density profile is complex. It is not exponential in the time, associated effective plasma diffusivity is strongly inhomogeneous across the pellet deposition zone and it is different before and after pellet injection. Another complication is that the "natural plasma density" $n_{e,N}$ (the density established by gas puffing and beam fuelling) is much a larger fraction of the plasma density in present-day plasmas than expected in a reactor. Figure 4 shows the pellet retention time τ_{pel} as a function of pellet deposition radius which is defined as the radius of maximum density perturbation by the pellet. The parameter τ_{pel} is determined from the equation $n_e(t, \rho_{pel}) - n_{e,N}(t, \rho_{pel}) \propto e^{-(t - t_{pel})/\tau_{pel}}$ by a log-linear regression using density profiles

measured by 200Hz Thomson scattering. Here t_{pel} is the time point just after the pellet deposition and $n_{e,N}(t,\rho_{pel})$ is the "natural density" linearly extrapolated from the pre-pellet time interval. The error bars measure the goodness of exponential fit. Values of τ_{pel} correlate with the status of the edge transport barrier, L-modes having the poorer particle confinement while extremely good confinement is found in ELM-free H-modes. It is also seen that for L-modes and ELMy H-modes the retention time τ_{pel} decreases for decreasing pellet penetration, perhaps even faster than for an effective diffusion coefficient, $D_{eff} = \left(a - r_{pel}\right)^2 \big/ 2\tau_{pel}$. In order to obtain useful scalings the anomalous particle transport is usually normalised to the heat transport [12], i. e. introducing the Prandtl-Peclet number. Figure 5 shows τ_{pel} normalised the to global energy confinement time $\tau_{E,tot}$ for relevant regimes, L-mode and ELMy H-modes. Similarly to τ_{pel} the ratio $\tau_{pel}/\tau_{E,tot}$ also decreases rapidly for shallower pellets.

Pellet retention has been simulated by the CUTIE code. For the discharge in figure 3 the pellet retention time was found to be $\tau_{pel} \approx 4.5ms$ ($\tau_{pel}/\tau_E \approx 0.2$), in good agreement with the data.

For pellet deposition expected in ITER, $r_{pel} \approx 0.80a$, the data in figure 5 extrapolate to $\tau_{pel}/\tau_{E,tot} \sim 0.2$. Pellet particle throughput required in a nominal ITER discharge [13] therefore has to be: $\Phi_{pel} = (n_e - n_{e,N})S(a - r_{pel})/\tau_{pel} = 74Pa\,m^3/s$, here $n_{e,N} = 0.5n_e$ (say), $n_e = 10^{20}m^{-3}$, the plasma surface is $S = 683m^2$ and the energy confinement time $\tau_E = 3.7s$. Such pellet throughput is about 75% of the present ITER design value [13]. Choosing even the largest envisaged pellet (5mm) implies that the interval between pellets has to be much shorter than the pellet retention time: $f_{pel} = 4Hz \sim 3/\tau_{pel}$. Such conditions are rare in present pellet fuelled plasmas. Further improvement of the scaling for τ_{pel} will require normalisation to the energy confinement time evaluated at the pellet deposition radius, analogous to the definition of pedestal energy confinement time in two term scaling law [14].

Acknowledgement. This work was funded jointly by the United Kingdom Engineering and Physical Sciences Research Council and by the European Communities under the contract of Association between EURATOM and UKAEA. The views and opinions expressed herein do not necessarily reflect those of the European Commission.

[1] Polevoi A. et al., 2003 Nucl. Fusion **43** 1072
[2] Baylor L. et al., 2007 Nucl. Fusion **47** 443
[3] Axon K. et al., 2004 Proc 31st EPS Conf. on Contr., Fus., London, ECA **28G**, P4.197
[4] Garzotti L. et al., 1997 Nucl. Fusion **37** 1167
[5] McNeill D. H., et al., 1991 Phys. Fluids **B 3** 1994.
[6] Lengyel L. L. 1977 Nucl. Fusion **17** 805
[7] Rozhansky V. A. et al., 1995 Plasma Phys. Contr. Fusion **37** 399
[8] Pegourie B., Garzotti L. 1997 Proc. 24th EPS Conf. on Contr., Fus., ECA **21A** 153
[9] Roach C. M. et al., 2005 Plasma Phys. Control. Fusion **47** B323
[10] Thyagaraja A. et al., 2005 Phys. Plasmas **12** 090907
[11] Garzotti L. et al., 2006 Nucl. Fusion **46** 73
[12] Valovič M. et al. 2007 Nucl. Fusion **47** 196
[13] ITER Final Design Report 2001, http://www.iter.org/a/index_nav4.htm
[14] Cordey J. G. for the ITPA H-mode Database Working Group, 2003 Nucl. Fusion **43** 670

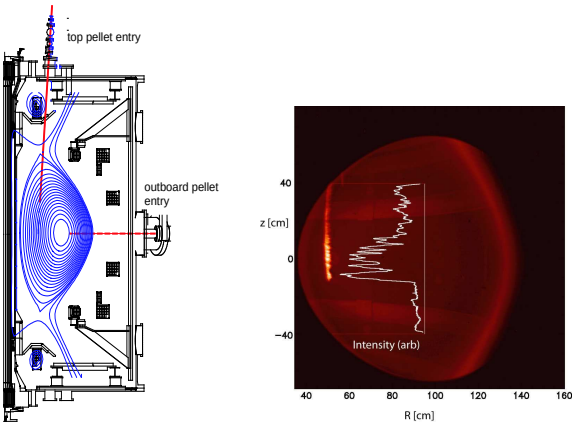

Figure 1. (a) left: the geometry of pellet injection. (b) right: The pellet image in narrow band visible bremsstrahlung (exposure is 7ms). The insert shows the emission intensity along the pellet trajectory.

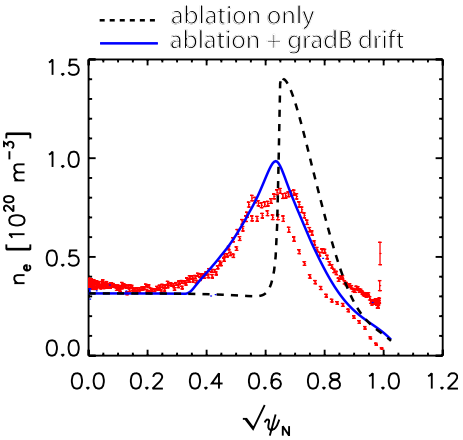

Figure 2. Red symbols: density profile at the end of pellet deposition captured by pellet-triggered Thomson scattering. Inboard and outboard profiles measured at the same time are shown. Black dashed line: prediction by NGPS model. Blue line: prediction by NGPS model with ∇B-drift.

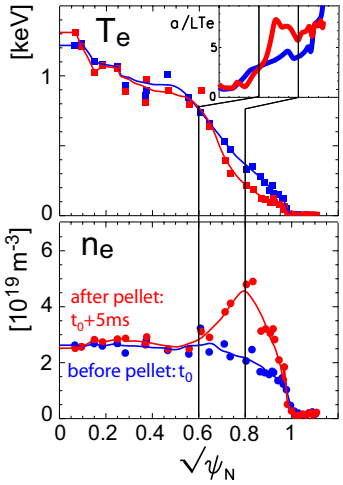

Figure 3(left) Electron temperature, T_e,and electron density, n_e, profiles before (blue) and after (red) the pellet injection as measured by 200Hz Thomson scattering system. The insert panel shows the normalised electron temperature gradient a ∇lnT_e over a small range of minor radius as indicated. The shot is ELMy H-mode, pulse number is 16335.

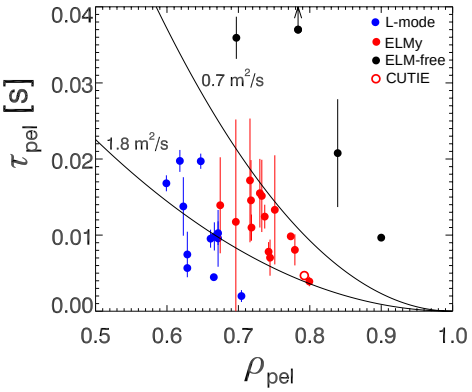

Figure 4. Pellet retention time τ_{pel} plotted against the normalised radius $\rho_{pel} = \sqrt{\psi_{N,pel}}$ taken at the maximum of the density perturbation by the pellet. The lines are the curves $\tau_{pel} = (a - r_{pel})^2 / 2D_{eff}$ for two values of effective diffusivity D_{eff} .

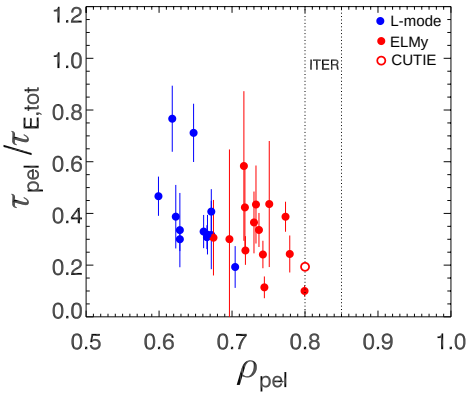

Figure 5. Pellet retention time normalised to total energy confinement time $\tau_{pel}/\tau_{E,tot}$ plotted against the pellet deposition radius as defined in figure 4.